Resonantly-initiated quantum trajectories and their role in the generation of near-threshold harmonics

Seth Camp,^{1,*} Samuel Beaulieu,^{2,3} Kenneth J. Schafer,¹ and Mette B. Gaarde^{1,†}

¹Deparment of Physics and Astronomy, Louisiana State University, Baton Rouge, Louisiana 70803-4001 ²Université de Bordeaux-CNRS-CEA, CELIA, UMR5107, F33405 Talance, France ³Institut National de la Recherche Scientifique, Centre EMT, J3X1S2, Varennes, Quebec, Canada (Dated: June 13, 2018)

We present a theoretical study of the role that resonant enhancement plays in the temporal and spectral properties of near-threshold harmonics in argon, driven by a moderately intense, nearinfrared laser pulse. By studying how the temporal profile of the eleventh harmonic (H11) changes with peak intensity and pulse duration, we show that H11 is predominantly emitted when the instantaneous intensity of the laser pulse is such that a high-lying excited state is Stark-shifted into multiphoton resonance with the ground state. We demonstrate that if this resonant intensity is lower than the peak intensity, the harmonic pulse will in general exhibit two peaks in time, on the rising and falling edges of the laser pulse. The resonantly enhanced harmonic radiation exhibits strong characteristics of semi-classical long and short quantum paths, and in general both paths are enhanced by the resonance. We find that the resonant enhancement leads to the harmonic radiation being emitted between .5 and 1.1 optical cycles after the time of multiphoton resonance, indicating that the resonance introduces a delay as compared to non-resonant emission. We further demonstrate that the resonantly-enhanced long-trajectory contribution to the harmonic radiation manifests in the spectral domain as red- and blueshifted features near the central harmonic frequency. Finally, we compare the single argon atom response to the macroscopic response of an argon gas and show that spectral and temporal effects of the resonance are still recognizable after propagation.

PACS numbers: 42.50.Hz, 42.65.Ky, 32.80.Rm

I. INTRODUCTION

High harmonic generation (HHG), which results from the interaction of an intense infrared (IR) laser pulse and a gas of atoms or molecules, is currently the primary source of coherent, tabletop extreme ultraviolet (XUV) radiation [1–4]. The generation process can be understood in a semi-classical recollision picture, whereby (i) laser-driven tunnel ionization creates an electron wave packet outside of the atomic core, (ii) the free electron wave packet accelerates in the laser field, and (iii) rescatters on the parent ion. The coherence between the returning electron wave packet and the ground state gives rise to emission of dipole radiation, with photon energies determined by the electron kinetic and potential energy at the time of recollision [5, 6].

The recollision picture has been essential in the use of HHG as a spectroscopic tool to study atomic and molecular structure and dynamics using harmonics well above the ionization threshold [7–14]. There is, however, growing interest in studying harmonics with energies around the ionization threshold of the generating atom [9, 15–30], an energy regime where the recollision picture, which de-emphasizes the interaction of the electron wave packet with the atomic potential, can be expected to break down [17–21, 24, 27, 31–33]. Recently, experimental and theoretical studies have observed that new spectral features

can appear in the high harmonic spectrum around threshold, features that do not fit within the basic three-step recollision picture [24, 28]. These new spectral peaks appear redshifted from the central harmonic frequency, with the magnitude of the shift depending on the driving wavelength and intensity. Beaulieu et al. demonstrated that these redshifted spectral features were related to harmonic emission occurring several optical cycles (O.C.) after the peak of the driving laser pulse and that they were directly related to atomic resonances driven by the laser-atom interaction [24]. It has been suggested that these new spectral features are related to HHG driven by electrons ionizing from excited states and then returning to the atomic core [24, 28], however, the exact mechanism driving this resonant interaction and the subsequent near-threshold harmonic emission is currently not fully understood.

In this paper, we investigate the role that resonances can play in the generation of near-threshold harmonics at moderate laser intensities, and their influence on the appearance of new features in the HHG spectrum of these harmonics. In particular, we study how resonantly enhanced high harmonic generation (REHHG), driven by multiphoton resonances between the ground state and Stark-shifted excited states, influences the temporal and spectral profile of these near-threshold harmonics. We solve the time-dependent Schrödinger equation (TDSE) for an argon atom in the single-active electron (SAE) approximation [34] for wavelengths between 770 and 870 nm and peak intensities between 20 and 60 TW/cm². In this paper we concentrate on identifying enhancement

^{*} scamp1@lsu.edu

[†] gaarde@phys.lsu.edu

features of harmonic 11 (H11) associated with particular resonances, although we have in general observed similar features for H7 through H15. At driving wavelengths and peak intensities where these Stark-shifted resonances occur at intensities below the peak intensity, we observe the appearance of both redshifted and blueshifted spectral features around the central harmonic frequency. By studying how the temporal profile evolves with peak intensity, pulse duration, and wavelength, we directly relate the appearance of these new spectral features to the temporal profile of H11. We find that the emission splits into an early and late contribution, with emission between .5 and 1.1 O.C. after the resonant intensity in the pulse envelope. We observe that this temporal splitting can be recognized also at the subcycle time scale, giving an intuitive physical picture of a process where the Starkshifted resonance helps in the initiation of long and short quantum trajectories that return with energies corresponding to H11 and nearby harmonics. In this physical picture, we interpret the peaks centered on the harmonic frequencies as resulting from resonantly initiated short quantum paths, and the red- and blueshifted features as resulting from resonantly initiated long quantum paths. In the latter case, the frequency shift is consistent with the variation of the accumulated semi-classical phase on the rising and falling edges of the pulse [24, 25, 35–39]. Finally, we calculate the macroscopic harmonic response and demonstrate that our single atom findings are still recognizable after propagation.

The paper is structured as follows: Section II gives an introduction to the numerical techniques applied in this paper. In Section III we discuss how to identify and characterize resonant enhancements in the single atom spectrum, by varying the intensity and wavelength of the driving field. In Sec. IV, we study the temporal profile of H11, both on the envelope and subcycle level, as a function of intensity and wavelength. In Sec. V, we map the temporal response of H11 back to the spectral profile of H11, interpreting the central harmonic feature and the red- and blueshifted spectral features in terms of resonantly initiated quantum trajectories. Section VI examines the results of our macroscopic calculations and Sec. VII presents a summary of our findings.

II. THEORETICAL METHOD

In this work, we use numerical methods very similar to those discussed previously in [23, 34]. Briefly, we solve the TDSE for an argon atom interacting with an intense laser field in the SAE approximation. We use a pseudopotential that closely replicates the singly excited state energies and oscillator strengths of argon [40]. Note that in this work we generally refer to the $3s^23p^5ns$ and $3s^23p^5nd$ excited states as ns and nd, respectively, and that for $n \geq 5$, every ns state has a corresponding (n-2)d state that occurs at approximately the same energy. Working in time units of O.C., we model the laser

as a cosine squared pulse in the form:

$$E_L(t) = E_0 \cos(\frac{c_2 t}{\tau})^2 \cos(2\pi t),$$
 (1)

where E_0 is the peak electric field, $c_2 = 2\arccos(\frac{1}{2}^{\frac{1}{4}})$, τ is the full width at half-maximum (FWHM) of the pulse, and the total pulse duration is given by $\frac{\pi\tau}{c_2}$ [41]. We calculate the dipole spectrum using the time-dependent acceleration, a(t), as $\widetilde{D}(\omega) = -\widetilde{A}(\omega)/\omega^2$, where the acceleration spectrum is given by:

$$\widetilde{A}(\omega) = \int a(t)W_H(t)e^{i\omega t}dt,$$
 (2)

and $W_H(t) = 0.5(1 + \cos(\frac{\pi t}{\tau_H}))$ is a Hanning window function [42] that smoothly brings the time-dependent acceleration to zero at the end of the time integration. As has been discussed previously [23, 43, 44], it is necessary to include a window function on a(t) in numerical calculations to act as an artificial lifetime on the excited states by ending any coherence between the ground state and population left in the excited states at the end of a calculation. For most of this paper, τ_H is chosen to bring the window function to 0 at the end of the laser pulse, allowing us to consider only the coherent, driven response of the atom to the laser pulse. However, in Sec. III we use a larger τ_H for times after the peak of the pulse, allowing the observation of narrow spectral features corresponding to population trapped in excited states at the end of the pulse. We use these narrow spectral features as "fingerprints" for field-driven electronic interactions with Stark-shifted excited states [23, 45, 46].

For the macroscopic calculations, we use the methods discussed in detail in [23, 47–50] to solve simultaneously the coupled Maxwell wave equation (MWE) and TDSE for a laser pulse propagating through a macroscopic gas of argon atoms. We use a focused (Gaussian) laser beam with a confocal parameter of .5 cm, and a focus located .25 cm before a .5-mm-long gas jet with a pressure of approximately 8 Torr. The temporal profile of the initial laser pulse and the intensity range (at the center of the gas) are the same as those used in the single atom calculations.

III. REHHG IN ARGON

In this section, we identify resonant enhancements in near-threshold harmonics of argon by examining how the HHG spectrum varies as a function of laser wavelength and peak intensity. A resonant enhancement occurs when a bound state is Stark-shifted into a multiphoton resonance with the ground state and the harmonic at the resonant energy, or a nearby harmonic, has a corresponding increase in its yield [23, 51–53]. This resonance condition can be expressed as:

$$\delta + \Delta E_s = q\omega, \tag{3}$$

where δ is the energy difference between the ground state and a field-free bound state, ΔE_s is the Stark shift imposed on the excited state by the field, q is an odd integer, and ω is the laser photon energy. When Eq. 3 is satisfied, harmonic q can be enhanced (direct resonant enhancement) and/or nearby harmonics can be enhanced (indirect resonant enhancement). As an estimate of the Stark shift we use $\Delta E_s = U_p$, where U_p is the ponderomotive energy [54] proportional to $I\lambda^2$ where I is the cycle-averaged intensity and λ is the driving wavelength. This is a good approximation for the higher lying states but tends to overestimate the Stark shift for the lowerlying states [21, 23, 45, 53, 55]. We note that $U_p=1.5~{\rm eV}$ for an intensity of 25 TW/cm² at 800 nm, meaning that for the intensities we consider in this paper, the Stark shift of excited states is at most a few eV. Most previous works on REHHG have in addition made the approximation of considering only enhancements occurring at the peak of the field by evaluating $\Delta E_s \approx U_p(I_0)$ in Eq. 3 using the peak intensity I_0 of the pulse. We will in general consider U_p to be a time-dependent function that varies with the intensity envelope of the pulse, meaning that the resonance condition can be fulfilled either at the peak of the pulse or on the rising and falling edges.

For the calculations shown in Fig. 1, the window-function characteristic time τ_H is longer for times after the peak of the laser pulse (t>0) than before. This means that the contribution to the dipole moment from excited states populated during the pulse is included for 30 O.C. after the end of the driving pulse, resulting in narrow spectral features at the field-free resonant frequencies of populated states, a signature of the occurrence of a multiphoton resonances during the pulse [23]. We consider a wavelength and intensity range so that Eq. 3 will be satisfied for the ns and (n-2)d states that are Stark-shifted into 11 photon resonance for $n \geq 5$ and the 4s state being Stark-shifted into 9 photon resonance.

Fig. 1(a) shows the HHG spectrum as a function of wavelength for a driving pulse with $\tau = 10$ O.C. and a peak intensity of 26.5 TW/cm². We observe that from 770 to 790 nm, there are no narrow spectral features at the bound state energies, aside from the 5s/3d state, which overlaps very closely with the ninth harmonic in this region. As the driving wavelength increases above 790 nm, a signal appears at the field-free energy of the 10s/8d state that transitions smoothly to lower energy with increased driving wavelength, reaching the 5s/3dstate at 870 nm. This shift of the signal from high-lying to low-lying states is consistent with these states Starkshifting into an 11 photon resonance with the ground state at the peak of the field. Similarly, the 4s state only appears as the wavelength is increased, consistent with a Stark-shifted, 9 photon resonance with the ground state. To confirm the relationship of this effect to the Starkshift, which depends on both wavelength and intensity, Fig. 1(b) shows harmonic spectra as a function of intensity, for an 800 nm, 10 O.C. pulse. When considering an intensity range that gives similar ponderomotive shifts,

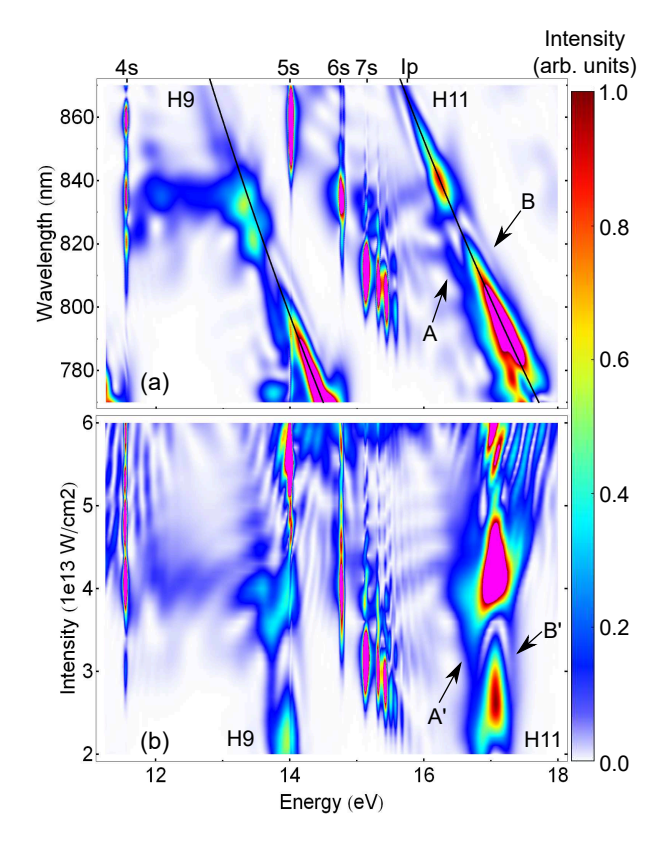


FIG. 1. (a) Harmonic spectra as a function of wavelength for a driving pulse with a peak intensity of $26.5~\mathrm{TW/cm^2}$ and $\tau=10~\mathrm{O.C.}$, for calculations using a Hanning window that lasts 30 O.C. after the end of the pulse. The solid black lines illustrate the wavelength-dependent locations of H9 and H11. The energies of the first 4 dipole-allowed excited states, along with the singly excited ionization potential, are indicated on the top axis. Arrows A and B highlight red- and blueshifted features appearing around the H11 central frequency. (b) Harmonic spectra as a function of intensity for the same pulse in (a), but for an 800 nm driving wavelength. Note each intensity has been rescaled for a better visual comparison of high and low intensity. Arrows A' and B' highlight red- and blueshifted features appearing around the central frequency of H11. Pink represents saturation of the scale.

one can indeed observe similar behavior: the remaining excited state population shifts from high-lying to lowerlying states as the intensity is increased.

We now turn our attention to the resonant enhancements related to these Stark-shifted resonances. We note that, interestingly, while Fig. 1(a) shows that many excited states have been (resonantly) populated, only two clear resonant enhancement features of H11 are evident in the figure: the first centered at approximately 800 nm when several states (8s/6d-10s/8d) near the ionization potential (I_p) are populated, and the second centered at approximately 835 nm when both the 4s and 6s/4d states are populated. The corresponding harmonic enhancements and excited state populations can be observed in Fig. 1(b) at approximately 27 TW/cm² and 40 TW/cm², respectively, and both Fig. 1(a) and (b) also show that

H9 is enhanced when H11 is enhanced, although to a lesser extent. We will see in the following section that the first enhancement feature agrees very well with the 9s/7d state (15.44 eV) being Stark-shifted into an 11 photon resonance. The second enhancement feature in H11 is harder to assign due to the 4s state (11.53 eV) being almost two photon resonant with the 6s/4d state (14.725 eV) in this wavelength regime. This means that when the 4s state shifts into a 9 photon resonance with the ground state, the 6s/4d state is close to an 11 photon resonance. Because of this ambiguity, we consider that this enhancement may be related to both features. Evaluating Eq. 3 at 800 nm, the 9s/7d resonance occurs at 26.5 TW/cm^2 , and the 4s (6s/4d) resonance occurs at $40.2 (38.5) \text{ TW/cm}^2$.

In Fig. 1(a) and (b), as the wavelength (intensity) is increased above the resonance condition for the 9s/7d state, we observe new red- and blueshifted spectral features that appear around the central harmonic frequency of H11 (labeled A (A') and B (B'), respectively). These features shift in energy as the pulse parameters are changed, but appear directly related to the harmonic frequency. We also observe similar features in the spectral profile of H9 at similar wavelengths and intensities, along with a redshifted feature appearing in Fig. 1 (a) around H11 at wavelengths (intensities) longer (larger) than resonant for the 4s and 6s/4d states. From the figure it is clear that these new spectral are related to the resonant enhancement of H11.

Beaulieu et al [24] experimentally observed similar redshifted spectral features in the intensity-dependent spectral profile of H13 in argon, which they related to resonant harmonic emission occurring several O.C. after the peak of the driving laser pulse. Here we have illustrated that these red- and blueshifted spectral features appear directly in relation to resonant enhancement features in the spectrum. In the next section we will relate these two observations by examining the temporal profile of H11 in the vicinity of these resonances.

IV. H11 TEMPORAL PROFILE

In this section we focus on the temporal profile of a resonantly enhanced harmonic as the peak intensity, pulse duration, and driving wavelength are varied. Fig. 2(a) shows the temporal profile of H11 as a function of driving intensity for an 800 nm, $\tau=10$ O.C. pulse. The profile has been calculated by applying a (narrow) 2ω -wide frequency window centered at H11 to the harmonic spectrum and then inverse Fourier transforming back to the time domain [23, 56, 57]. Note that the time profile has been normalized for each intensity to ease comparison of the harmonic yields from high and low intensity driving pulses, and the color scale is the same as in Fig. 1. We see that up to approximately 26.5 TW/cm² (the intensity of the observed H11 resonant enhancement by the 9s/7d state), the harmonic pulse is shorter than the

driving pulse and has a single peak. This is in general what one would expect for the temporal behavior of a highly nonlinear process such as HHG. As the intensity increases, however, the time profile branches into two distinct pieces: one early in the pulse, and one late in the pulse. This branching of the time profile is asymmetric about t=0 and dominates the response of H11 until approximately $40.2~\mathrm{TW/cm^2}$. In the previous section, we discussed that at this intensity, H11 is dominated by the resonant enhancement due to the dual 4s and 6s/4d resonances. Near this intensity we again find the appearance of a single dominant peak in the temporal profile that branches into an early and late contribution as the peak

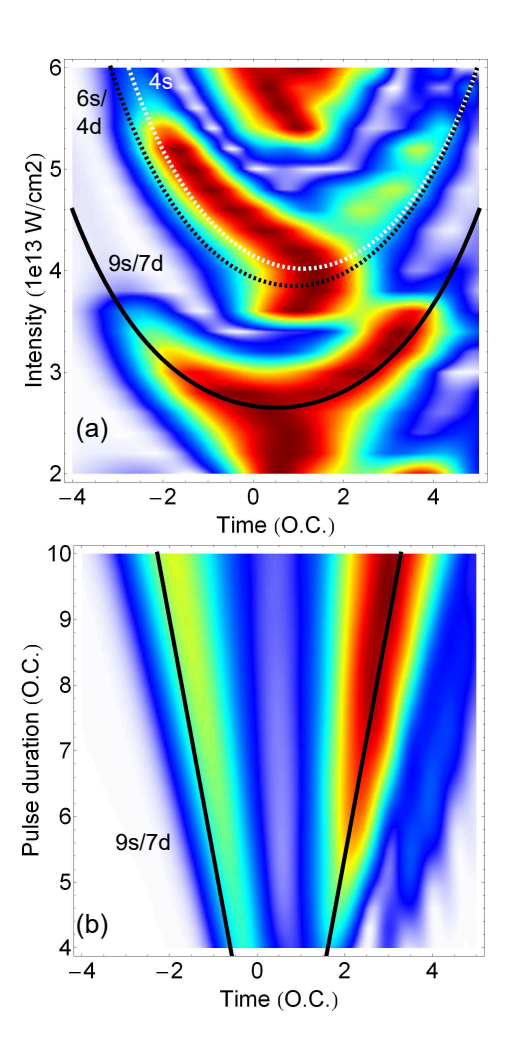


FIG. 2. (a) Temporal profile of H11 as a function of intensity in argon for an 800 nm, $\tau=10$ O.C. pulse. Overlaid with curves representing constant intensities of 26.5 TW/cm² (solid), 38.5 TW/cm² (black, dashed), and 40.2 TW/cm² (white, dashed) shifted in time by .5, .9, and 1.1 O.C., respectively. Note, each intensity calculation has been normalized to a maximum of 1 for ease of comparison between high and low intensities. (b) Temporal profile of H11 as a function of pulse duration for an 800 nm, $I_0=32.5$ TW/cm² pulse. Overlaid with curves representing a constant intensity of 26.5 TW/cm², shifted by .5 O.C.

intensity increases.

Fig. 2(b) shows how the H11 time profile changes as a function of pulse duration for an 800 nm, 32.5 TW/cm^2 pulse. The peak intensity is such that H11 is dominated by the resonant enhancement due to the 9s/7d state, and the time profile is already split into two branches, which shift linearly to earlier and later times as the pulse duration increases.

Both Fig. 2(a) and (b) demonstrate how profoundly the time profile is influenced by the resonant enhancement. The generation of H11 is a highly nonlinear process, which in the absence of the resonances would happen near the peak of the driving laser pulse. As explained in more detail below, the enhancement provided by the (Stark-shifted) resonance is so strong that when the resonance condition is met on the rising and falling edge of the pulse, the time profile is dominated by the emission at these two times rather than at the peak of the laser pulse.

We can model the time dependence of the resonant enhancement by allowing Eq. 3 to be satisfied at times during the pulse other than t=0. While it has not been explored in terms of REHHG, it has been previously demonstrated that Stark-shifted multiphoton resonances can occur away from the peak of the pulse and be explained by considering U_p in Eq. 3 to be time-dependent, rather than set by the peak intensity of the pulse [58, 59]. We thus assume that $U_p(t) \propto I_0 \cos^4(\frac{c_2 t}{\tau})\lambda^2$. For a fixed λ , q, and E_i , Eq. 3 will still be satisfied by only a single resonant intensity, however, pulses with peak intensities larger the resonant will cross the resonant intensity twice; on the rising and falling edges of the pulse. For a pulse width τ and a given resonant intensity I_r , we can identify the resonance times t_{\pm}^r from:

$$I_r = I_0 \cos^4\left(\frac{c_2 t_{\pm}^r}{\tau}\right),\tag{4}$$

which leads to

$$t_{\pm}^{r} = \pm \frac{\tau}{c_2} \arccos\left(\sqrt[4]{\frac{I_r}{I_0}}\right).$$
 (5)

where + (-) represents the rising (falling) intensity edge of the pulse. Eq. 5 defines curves of constant intensity in the (t, I_0) and (t, τ) parameter spaces, and defines the times at which this resonant intensity is met.

We find that Eq. 5 reproduces the resonant emission patterns in Fig. 2(a) and (b) well, provided that we shift them in time by 0.5-1 O.C. to account for the difference between the "excitation time" (given by the resonance condition), and the emission time, which happens later. This is demonstrated by the black solid curves that are overlaid on Fig. 2(a) and (b), which correspond to an emission time of .5 O.C. after the 9s/7d resonant intensity of 26.5 TW/cm². In Fig. 2(a), we also overlay dashed lines representing resonant intensities of 38.5 TW/cm² (black) shifted by .9 O.C. and 40.2 TW/cm² (white) shifted by 1.1 O.C., representing the 6s/4d and

4s resonances, respectively. In both Fig. 2(a) and (b), the agreement between the curves and the observed temporal profile is very good [60]. This agreement motivates a number of conclusions: (i) the observed temporal splitting of H11 is indeed related to harmonic enhancement through resonances whose "initiating" intensity varies in time as we alter the peak intensity and pulse duration, (ii) the delay between the excitation time and the emission time is consistent with the picture of resonantly initiated quantum paths, i.e., that the main influence of the resonance is to assist in promoting the electron out of the ground state, after which it will follow semi-classical trajectories as in non-resonant above threshold HHG. In non-resonant above threshold HHG, the delay between excitation and emission depends primarily on the quantum path and generally varies between zero and one optical cycle, with an average of approximately 0.7 O.C. for low energy harmonics if both quantum paths contribute equally [23, 35, 36].

Interestingly, as the peak intensity is raised, the temporal profile of a single resonance seems to follow it into the temporal wings of the driving pulse until a new state begins to come into resonance around the peak of the pulse. For example, the emission around t=0 at the highest intensities in Fig. 2(a) actually corresponds to the 5s/3d state coming into multiphoton, Stark-shifted resonance with H11. This again serves to demonstrate that for these parameter ranges, the temporal dynamics of near-threshold harmonics can be almost entirely dependent on these harmonic resonances. Also note that the distinctive and consistent temporal shifts related to the different resonances in Fig. 2 (a) suggests that each resonance initiates continuum dynamics that are unique to that resonance, with the return time depending only on which particular resonance is being driven.

Looking in more detail at Fig. 2(a) we see that there can also be differences between the emission initiated on the rising vs. the falling edges of the pulse. For the 9s/7dresonance, the emission on the falling edge is stronger than that on the rising edge. The 6s/4d resonance, on the other hand, shows a particularly strong asymmetry, with a well-defined early emission peak and a much weaker, late emission peak that appears to exhibit effects of interference, given its semi-periodic variation with the peak intensity. Possible sources of this interference are that both the 4s and the 6s/4d states are shifted into resonance (9 and 11 photons, respectively), and/or that population that was resonantly transferred to the excited state on the rising edge of the pulse also contributes to the signal on the falling edge of the pulse for this particular resonance(s).

Fig. 3 shows the H11 temporal profile as a function of driving wavelength in a range covering the dual 4s and 6s/4d resonance. For fixed I_0 and τ , increasing λ will lower the intensity necessary to drive the resonance, moving the resonant intensity into the temporal wings of the pulse for fixed peak intensity. Fig. 3 has been overlaid with the λ -dependent time of the resonant intensity for

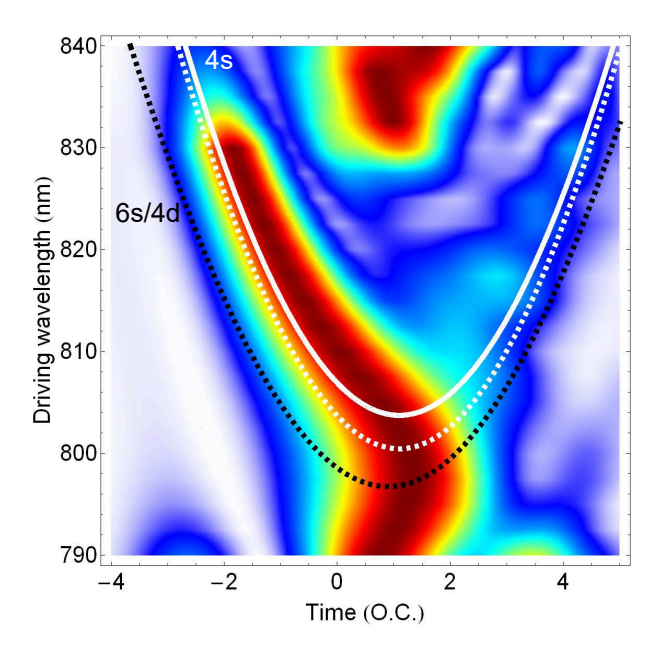


FIG. 3. The temporal profile of H11 as a function of wavelength in argon for a $\tau=10$ O.C. and $I_0=40$ TW/cm² pulse. We overlay the plot with curves of the λ -dependent time of the resonant intensity for an indirect enhancement of H11 by a 9-photon, 4s resonance, shifted by 1.1 O.C., with a ponderomotive Stark-shift (white, dashed), a Stark-shift 4% smaller (white, solid), and a direct enhancement of H11 by a 11-photon, 6s/4d resonance, shifted by .9 O.C. Here the temporal profile at each wavelength has been normalized to a maximum value of 1.

the 4s (white, dashed) and 6s/4d (black, dashed) states, shifted 1.1 and .9 O.C., respectively. In this case almost the same structure is observed as when varying the peak intensity, with the same asymmetry between emission on the rising and falling edges of the pulse. The similarity between the asymmetry as a function of I_0 and λ is interesting, because these comparable processes are occurring for otherwise very different parameters: different ponderomotive shifts, intensities, times, and wavelengths, and yet, the emission signatures on the rising and falling edges are very similar. This seems to further imply that the electron dynamics initiated by REHHG are less dependent on the specific pulse parameters, and more dependent on the fact that a particular resonance is driven with either a rising or falling intensity. Also note that the enhancement feature occurs slightly above both dashed curves (as can also be seen in Fig. 2(a) for this resonance), suggesting that the responsible state shifts slightly less than ponderomotively. To emphasize this further, the plot has also been overlaid with a resonant curve for the 4s state using $.96U_p$ for ΔE_s (white, solid), resulting in better agreement with the numerical result. Similarly good agreement can be obtained for the 6s/4dresonance by reducing the Stark-shift to approximately $.9U_p$.

It is worth noting here that we have observed this type

of single-to-multiple peak branching of the temporal profile for a range of harmonics (H7-H15) near threshold in argon, as a function of wavelength and as a function of intensity, similar to the behavior shown in Figs. 2 and 3. This branching in general happens at slightly different intensities and wavelengths for different harmonics, indicating that different resonances can play a dominant role for different harmonics. Likewise, we have observed similar behavior of near-threshold harmonics in helium (H7-H13), generated with wavelengths ranging between 400-500 nm. Although we have not analyzed these harmonics in Ar and He in as much detail as H11 discussed in this paper, these observations strongly suggest that for moderate intensities, near-threshold harmonics in general exhibit strong characteristics of resonant enhancement.

We next investigate the subcycle behavior of the harmonic radiation in the vicinity of the 9s/7d resonance. Fig. 4(a) shows the time-profile of a 12ω wide spectral range centered on H11, generated by an 800 nm, $\tau = 10$ O.C. pulse for an intensity range covering the 9s/7d resonance. The dotted line in each plot shows the time profile of H11 only, calculated with a much narrower window. There is generally good agreement between the envelope of the H11 time profile and that of the larger range, with both splitting primarily into an early and late contribution, indicating that several of the nearby harmonics are influenced by the resonance in a fashion similar to that of H11. Interestingly, note that as the broadband time profile splits into early and late contributions, one can still recognize the two emission peaks per half cycle that are traditionally associated with the short and long trajectory returns. By considering the full time-frequency profiles such as shown in Fig. 4(b) and (c), one can identify that the short-trajectory bursts are generally stronger than the long-trajectory bursts.

Fig. 4(b) and (c) show the time-frequency profiles for the 32.5 TW/cm² case shown in (a), for times around the peak emission on the rising and falling edges, respectively. At these times, as discussed above, the harmonic emission is dominated by the resonant enhancement provided by the Stark-shifted 9s/7d resonance. The fact that the subcycle time profile clearly shows evidence of what looks like short and long trajectories strongly supports the idea that the main effect of the resonance is to help initiate the HHG process, and that once the electron has been excited out of the ground state, it will follow the usual semi-classical dynamics. With our previous observation of asymmetries between the emission profiles for the rising and falling edge of the laser pulse, this opens the door to potentially using the temporal profiles around a resonance to gain greater insight into the ionizing and returning electron dynamics. For example, an open question is whether the delay between excitation and emission, which as discussed above seems to be characteristic of each resonance, happens predominantly in the excitation or the recombination step. In particular, can the delay be interpreted as the excited state "holding on" to the initially ionized electron before launching it on

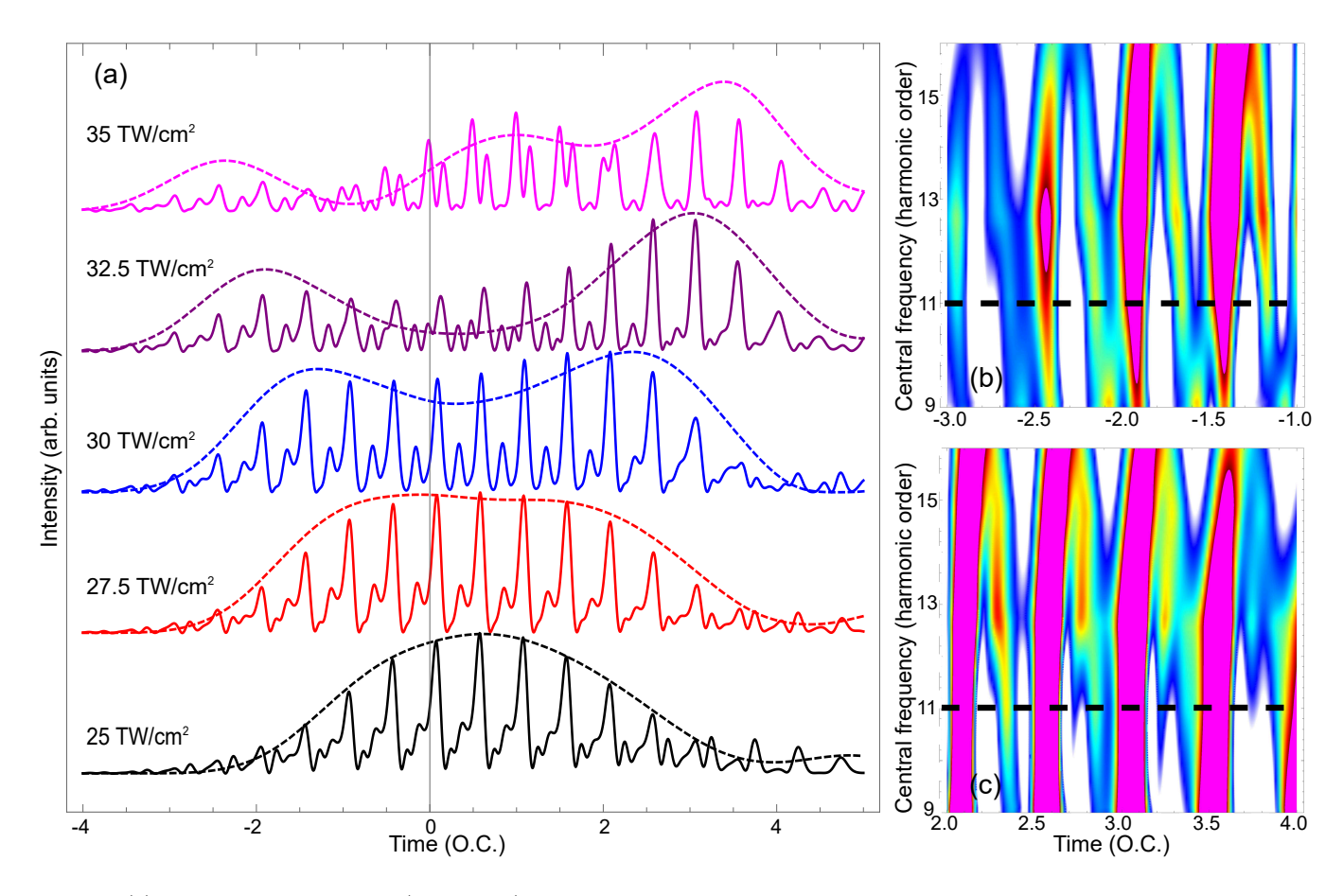


FIG. 4. (a) Subcycle time profiles (solid lines) of the harmonic subcycle radiation calculated using a spectral width from H5-H17, centered on H11, for different peak intensities of an 800 nm, $\tau=10$ O.C. pulse. Also shown (dashed lines) are the corresponding H11 time profile. Each intensity profile is normalized to a maximum of 1. (b) Time-frequency profile of the broadband harmonic radiation at an intensity of 32.5 TW/cm^2 centered around the peak on the rising edge. The thick dashed line represents the location of the line-out shown in (a), second plot from the top. (c) Same as (b), except centered around the peak on the falling edge.

a semi-classical trajectory or after it returns to the vicinity of the core (the latter being similar to the four-step model proposed in [61], for which the subsequent time-frequency profile results have been explored in [62])? Or should it be interpreted as a phase shift due to propagation in the atomic potential, similar to the Wigner time delay [63]? To address such questions one would have to be able to compare the exact quantum trajectories the ionized electron would be expected to follow in the absence or presence of the resonant enhancement, which is clearly non-trivial.

V. SPECTRAL SIGNATURES OF RESONANTLY INITIATED TRAJECTORIES

We next explore the consequences of the characteristic temporal behavior of REHHG in the spectral domain. This will allow for better comparison with experiments, where harmonics are usually characterized by their spectral behavior [21, 22, 24, 25, 27]. Fig. 5(a) and (b) show

the spectral profiles around H11 as a function of intensity and pulse duration, for intensities near the 9s/7d resonance. The laser parameters are the same as those used for the H11 temporal profiles shown in Fig. 2(a) and (b).

Fig. 5(a) and (b) show that the resonantly enhanced spectra split into three distinct peaks for most intensities and pulse durations. We can understand this behavior by considering the (well known) time-dependent phase that is acquired by each harmonic during the laser pulse [24, 25, 35–39]. This phase, $\phi_q \approx \alpha_q^{s,l} U_p/\omega$, is acquired by the electron wave packet each laser cycle while it propagates in the continuum. The phase is thus proportional to the laser intensity as it varies during the pulse. The phase coefficients $\alpha_q^{s,l}$ (which are different for each harmonic) are characteristic of how long the electron spends in the continuum and are quite different for the short and long trajectory contributions. For the lowest energy harmonics (just above threshold), the semi-classical model predicts that $\alpha_q^s \approx 0$ and $\alpha_q^l \approx 2\pi$ [36], and the spectral characteristics of the short- and long-trajectory contribution to each harmonic are thus very distinct, since the

spectral broadening caused by the time-dependent phase is much larger for the long-trajectory contribution than for the short [47, 48, 56, 64–66].

The combination of the time-dependent phase and the fact that resonantly enhanced harmonics are emitted primarily at (or rather, shortly after) the two times of resonance during the pulse gives the characteristic spectra observed in Fig. 5(a) and (b). The short-trajectory contribution to the harmonic does not gain much phase and is therefore centered on the harmonic frequency. This can be seen as the strong spectral features centered on 11ω in Fig. 5(a) and (b). The long-trajectory contribution, however, is now split into two main contributions below and above the central frequency, corresponding to:

$$\omega_{11} = 11\omega + \alpha_{11}^l \left. \frac{d(U_p/\omega)}{dt} \right|_{t=t_s}, \tag{6}$$

where t_e is the time of emission, which for the 9s/7dresonance happens about .5 O.C. after the time of resonance on either the rising or falling edge of the pulse. The long trajectory yields one blueshifted and one redshifted peak in the spectrum, separated from each other and also from the short trajectory peak (in contrast to the non-resonant case in which the broad, long-trajectory contribution overlaps the narrow, short-trajectory contribution to the spectrum). In Fig. 5(a) and (b) we have overlaid curves that show the prediction for the instantaneous frequency of the long-trajectory contribution on the rising and falling edge of the laser pulse, according to Eq. 6, for different peak intensities and pulse durations. We use a value of $\alpha_{11}^l = 2.4\pi$ to get the best fit to the numerical results overall (for the shortest pulse durations, it is not a good approximation to consider only the time-dependence of the intensity to calculate the instantaneous frequency, see [67, 68]). The fact that $\alpha_{11}^l > 2\pi$ gives the best fit is consistent with previous experimental and theoretical findings for long-trajectory, below-threshold harmonics [19, 20] [69]. Finally, we note that the asymmetry of the two peaks with respect to the central frequency, observed in both the predicted curves and the numerical results, is due to the fact that the emission occurs later than the resonant intensity - this means that although the resonance conditions are symmetric in time around the peak, the emission time is not.

Figs. 5(a) and (b) also show that the strengths of the low-frequency and high-frequency peaks are different, consistent with the temporal behavior observed in Fig. 2(a) and (b) in which the 9s/7d resonance is emitted more strongly for the resonant burst in the falling edge of the pulse. Experimentally, there been one observation of redshifted peaks in the context of resonantly enhanced harmonics [24], and theoretically it has been discussed in [28], but there has been little to no discussion or measurement of blue shifted peaks. Our results suggest that the enhancements measured in [24] originated in resonances with a preference for emission on the falling edge of the pulse, similar to the 9s/7d resonance discussed above.

For completeness, let us note that although we do see

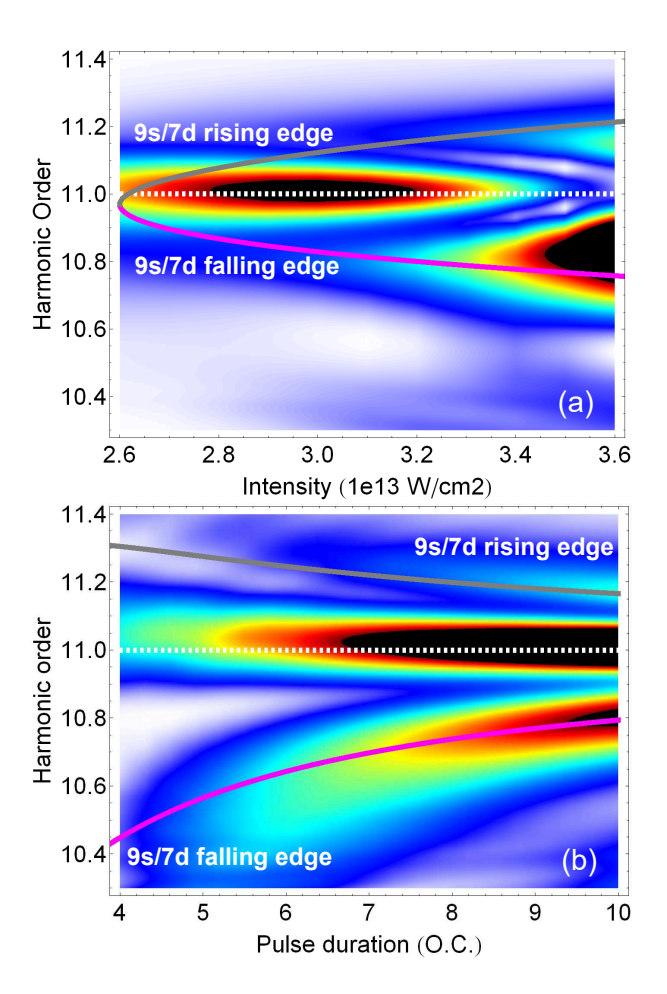


FIG. 5. (a) and (b) show the spectra corresponding to the temporal profiles in Fig. 2(a) and (b), respectively. The intensity range in (a) is chosen such that we only see the effect of the 9s/7d resonance. The solid curves represent the instantaneous frequency expected from the 9s/7d resonantly enhanced long-trajectory contribution on the rising (grey) and falling (purple) edges, see Eq. 6. The α value here corresponds to 2.4π rad. The color scale is chosen such that parts of the spectra are saturated (black), in order to show the weaker spectral features.

strong evidence of resonantly enhanced quantum-path contributions to H11, we cannot exclude that there could be additional, non-trajectory-driven, contributions to the harmonic emission. The peaks in the sub-cycle time profiles in Fig. 4 are often broad and could be representing a mix of quantum-path and (for example) perturbative behavior. In the spectral domain, the latter contribution would likely appear near the central frequency and would be difficult to separate from the short-path contribution.

VI. MACROSCOPIC RESPONSE

Finally, we consider the macroscopic harmonic response of a gas of argon atoms for similar conditions as discussed above. Fig. 6(a) and (b) show the macro-

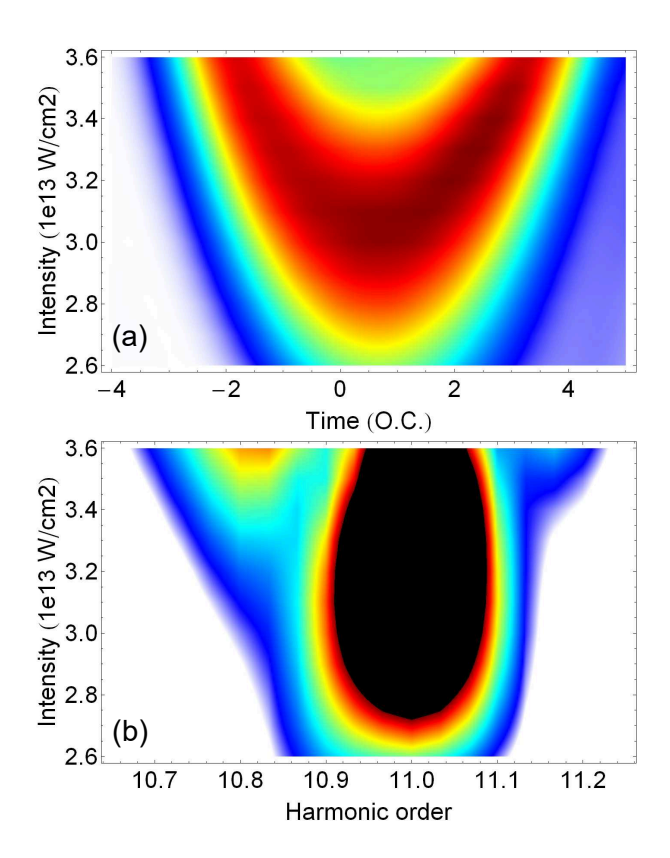


FIG. 6. Macroscopically calculated temporal (a) and spectral (b) profiles for H11, using an 800 nm, 10 O.C. laser pulse focused one Rayleigh range (2.5 mm) before the center of the gas. The intensity indicated on the vertical axis is the intensity in the center of the gas jet.

scopic temporal and spectral profile of H11 as a function of the peak intensity at the center of the gas for an 800 nm, 10 O.C. laser pulse. The macroscopic response has been spatially filtered by projecting the electric field at the end of the medium into the far field, selecting only the emission near the central axis, and then backtransforming to the near field. We then plot the radially integrated temporal or spectral yield. This is equivalent to the spatial filtering used in many experiments in the form of a small aperture in the far field. In both Fig. 6(a) and (b), we find very good agreement with the corresponding single atom results shown in Fig. 2(a) and Fig. 5(a). Volume averaging over the intensity distribution of the generating field leads to a small shift in both the temporal and spectral features as compared to the single atom results in Fig. 2(a) and Fig. 5(a). For the calculations in Fig. 6(a) and (b), the focusing conditions are such that the short trajectory contribution is favored by phase matching, since the laser focus is approximately one Rayleigh range before the center of the gas. Additionally, the spatial filter reduces the strength of the more divergent long-trajectory contribution relative to the short-trajectory contribution, as can be seen from the relative strength of the central and the shifted spectral features in Fig. 6(b). We find (not shown) that

focusing conditions in which the long trajectory contribution is favored generate similar results. This is consistent with previous macroscopic findings concerning the effect of phase-matching on resonantly enhanced features [23]. It is worth noting here that in the absence of the far field spatial filter, one can still recognize the red- and blueshifted features in the spectrum, although they are weaker and less distinct. Similarly, in the time domain the distinct two-peak structure is less visible without the far field spatial filter. We believe that both of these results are due to the effect of averaging over a number of intensities in the near field, which gives rise to enhancement at different times during the pulse, thereby washing out the intensity-specificity of the single atom results. Finally, we remark that while the blueshifted feature is weak, it still persists. This suggests that this feature should be observable in experiments, even though it has not been seen to date.

VII. SUMMARY

We have studied the role that multiphoton, Starkshifted resonances play in the generation of nearthreshold harmonics in argon for moderate driving laser intensities. Our results suggest that there are regimes in which the temporal behavior of near-threshold harmonics is dominated by the resonantly enhanced response. In particular we have shown that the temporal and spectral profiles of H11 are dominated by the resonant response for intensities and wavelengths such that the 4s, 9s/7d, and 6s/4d states are Stark-shifted into multiphoton resonance with a near-threshold harmonic (H9 and H11). When the multiphoton resonance condition is fulfilled on the rising and falling edges of the driving laser pulse (rather than at the peak) this causes the harmonic temporal profile to split into two branches, each corresponding to harmonic emission taking place shortly after the time of the resonant intensity. This type of branching can be observed for a range of near-threshold harmonics (H7-H15). By studying the subcycle time profile, we have also shown that the resonantly enhanced harmonic radiation exhibits strong semi-classical characteristics, with two bursts per half-cycle similar to those of the short and long quantum path contributions familiar from nonresonant HHG. In the frequency domain, the combination of the temporal splitting of the harmonic envelope and the contribution of both short and long quantum paths leads to harmonic spectra with a strong central peak and both a red- and a blueshifted peak. The redand blueshifted peaks in particular are consistent with a long-path contribution, resonantly initiated on the rising or falling edge of the pulse. Finally, we showed that the temporal branching and spectrally shifted features are still prominent in the temporal and spectral profiles of H11 after propagation.

Our results support a picture of resonant enhancement as an enhancement of the first step in a semi-classical three-step model, i.e. that the multiphoton resonance aids in the initial excitation of the electron out of the ground state. After that, the electron follows semiclassical quantum paths in the continuum and returns with a total energy near or below the ionization threshold [19]. Interestingly, we find that the delay between the resonantly enhanced excitation and emission time, as measured by the peaks in the H11 temporal envelope, depends on the multiphoton resonance. In particular, we saw that the delay associated with the 9s/7d resonance is about 0.5 O.C. whereas that associated with the 4s and 6s/4d resonances is closer to 1 O.C. This suggests that another effect of the resonant enhancement is a phase shift on the excited and/or returning electron wave packet, which is characteristic of the resonance. Since this delay will be apparent in the magnitude of the spectral shift and asymmetry of the long path contribution to the harmonic spectrum, this may provide an experimental approach to further characterizing the role of resonances in REHHG. As an example, high-precision measurements employing the attosecond light house technique promise the ability to measure not only the temporal envelope but also the subcycle characteristics of resonantly enhanced harmonic emission [24]. Furthermore, we expect that the increasing access to high-repetition-rate laser sources, which allow for high-average-flux HHG using a moderate laser intensity, will in general lead to more studies in which resonantly-initiated quantum trajectories play an important role.

ACKNOWLEDGMENTS

This work was supported by the National Science Foundation under Grants No. PHY-1403236 and PHY-1713671. S.B. acknowledges support from a Vanier Scholarship. Portions of the research were conducted using high-performance computing resources provided by Louisiana State University (LSU HPC) and the Louisiana Optical Network Initiative (LONI).

- A. McPherson, G. Gibson, H. Jara, U. Johann, T. S. Luk, I. A. McIntyre, K. Boyer, and C. K. Rhodes, J. Opt. Soc. Am. B 4, 595 (1987).
- [2] M. Ferray, A. L'Huillier, X. F. Li, L. A. Lompre, G. Mainfray, and C. Manus, Journal of Physics B: Atomic, Molecular and Optical Physics 21, L31 (1988).
- [3] A. L'Huillier, D. Descamps, A. Johansson, J. Norin, J. Mauritsson, and C. Wahlstrom, Eur. Phys. J. D 26, 91 (2003).
- [4] F. Krausz and M. Ivanov, Rev. Mod. Phys. 81, 163 (2009).
- P. B. Corkum, Phys. Rev. Lett. 71, 1994 (1993).
- [6] K. J. Schafer, B. Yang, L. F. DiMauro, and K. C. Kulander, Phys. Rev. Lett. 70, 1599 (1993).
- [7] J. Itatani, J. Levesque, D. Zeidler, H. Niikura, H. Pépin, J.-C. Kieffer, P. B. Corkum, and D. M. Villeneuve, Nature 432, 867 (2004).
- [8] H. Wörner, J. Bertrand, D. Kartashov, P. Corkum, and D. Villeneuve, Nature 466, 604 (2010).
- [9] H. Soifer, P. Botheron, D. Shafir, A. Diner, O. Raz, B. D. Bruner, Y. Mairesse, B. Pons, and N. Dudovich, Phys. Rev. Lett. 105, 143904 (2010).
- [10] A. Shiner, B. Schmidt, C. Trallero-Herrero, H. Wörner, S. Patchkovskii, P. Corkum, J. Kieffer, F. Légaré, and D. Villeneuve, Nature Physics 7, 464 (2011).
- [11] M. Wong, A.-T. Le, A. Alharbi, A. Boguslavskiy, R. Lucchese, J.-P. Brichta, C. Lin, and V. Bhardwaj, Physical review letters 110, 033006 (2013).
- [12] M. Miller, A. Jaroń-Becker, and A. Becker, Physical Review A 93, 013406 (2016).
- [13] P. Lan, M. Ruhmann, L. He, C. Zhai, F. Wang, X. Zhu, Q. Zhang, Y. Zhou, M. Li, M. Lein, et al., Physical Review Letters 119, 033201 (2017).
- [14] S. Schoun, A. Camper, P. Salières, R. Lucchese, P. Agostini, and L. DiMauro, Physical Review Letters 118, 033201 (2017).
- [15] P.-C. Li, Y.-L. Sheu, C. Laughlin, and S.-I. Chu, Phys. Rev. A 90, 041401 (2014).

- [16] P.-C. Li, Y.-L. Sheu, C. Laughlin, and S.-I. Chu, Nature communications 6, 7178 (2015).
- [17] W.-H. Xiong, J.-W. Geng, J.-Y. Tang, L.-Y. Peng, and Q. Gong, Phys. Rev. Lett. 112, 233001 (2014).
- [18] K. N. Avanaki, D. A. Telnov, and S.-I. Chu, Journal of Physics B: Atomic, Molecular and Optical Physics 49, 114002 (2016).
- [19] J. A. Hostetter, J. L. Tate, K. J. Schafer, and M. B. Gaarde, Phys. Rev. A 82, 023401 (2010).
- [20] D. C. Yost, T. R. Schibli, J. Ye, J. L. Tate, J. Hostetter, M. B. Gaarde, and K. J. Schafer. Nat Phys 5, 815 (2009).
- [21] P. Ackermann, H. Münch, and T. Halfmann, Opt. Express 20, 13824 (2012).
- [22] M. Chini, X. Wang, Y. Cheng, H. Wang, Y. Wu, E. Cunningham, P.-C. Li, J. Heslar, D. A. Telnov, S.-I. Chu, et al., Nature Photonics 8, 437 (2014).
- [23] S. Camp, K. J. Schafer, and M. B. Gaarde, Phys. Rev. A 92, 013404 (2015).
- [24] S. Beaulieu, S. Camp, D. Descamps, A. Comby, V. Wanie, S. Petit, F. Légaré, K. J. Schafer, M. B. Gaarde, F. Catoire, et al., Physical review letters 117, 203001 (2016).
- [25] L. He, P. Lan, Q. Zhang, C. Zhai, F. Wang, W. Shi, and P. Lu, Physical Review A 92, 043403 (2015).
- [26] W.-H. Xiong, J.-W. Geng, Q. Gong, and L.-Y. Peng, New Journal of Physics 17, 123020 (2015).
- [27] W.-H. Xiong, L.-Y. Peng, and Q. Gong, Journal of Physics B: Atomic, Molecular and Optical Physics 50, 032001 (2017).
- [28] W.-H. Xiong, J.-Z. Jin, L.-Y. Peng, and Q. Gong, Physical Review A 96, 023418 (2017).
- [29] P. Mulholland and D. Dundas, arXiv preprint arXiv:1703.05245 (2017).
- [30] E. P. Power, A. M. March, F. Catoire, E. Sistrunk, K. Krushelnick, P. Agostini, and L. F. DiMauro, Nature Photonics 4, 352 (2010).
- [31] J.-C. Liu, M. C. Kohler, C. H. Keitel, and K. Z. Hatsagortsyan, Physical Review A 84, 063817 (2011).

- [32] J. Heslar and S.-I. Chu, Scientific reports 6, 37774 (2016).
- [33] J. Heslar and S.-I. Chu, Physical Review A 95, 043414 (2017).
- [34] K. J. Schafer, in Strong Field Laser Physics, edited by T. Brabec (Springer, New York, 2008).
- [35] M. Lewenstein, P. Balcou, M. Y. Ivanov, A. L'Huillier, and P. B. Corkum, Phys. Rev. A 49, 2117 (1994).
- [36] M. Lewenstein, P. Salières, and A. L'Huillier, Phys. Rev. A 52, 4747 (1995).
- [37] M. B. Gaarde, F. Salin, E. Constant, P. Balcou, K. Schafer, K. Kulander, and A. LHuillier, Phys. Rev. A 59, 1367 (1999).
- [38] P. Salières, A. L'Huillier, P. Antoine, and M. Lewenstein, Advances in Atomic Molecular and Optical Physics 41, 83 (1999).
- [39] C. M. Heyl, J. Güdde, U. Höfer, and A. LHuillier, Phys. Rev. Lett. 107, 033903 (2011).
- [40] J. Mauritsson, M. B. Gaarde, and K. J. Schafer, Physical Review A 72, 013401 (2005).
- [41] I. Barth and C. Lasser, Journal of Physics B: Atomic, Molecular and Optical Physics 42, 235101 (2009).
- [42] R. B. Blackman and J. W. Tukey, "The measurement of power spectra from the point of view of communications engineering," (1958).
- [43] H. Ahmadi, M. Vafaee, and A. Maghari, Journal of Physics B: Atomic, Molecular and Optical Physics 49, 035602 (2016).
- [44] M. Vafaee, H. Ahmadi, and A. Maghari, Journal of Physics B: Atomic, Molecular and Optical Physics 50, 025601 (2016).
- [45] S. Beaulieu, E. Bloch, L. Barreau, A. Comby, D. Descamps, R. Géneaux, F. Légaré, S. Petit, and Y. Mairesse, Physical Review A 95, 041401 (2017).
- [46] S. Bengtsson, E. Larsen, D. Kroon, S. Camp, M. Miranda, C. Arnold, A. L'Huillier, K. Schafer, M. Gaarde, L. Rippe, et al., Nature Photonics 11, 252 (2017).
- [47] M. B. Gaarde, J. L. Tate, and K. J. Schafer, J. Phys. B 41, 132001 (2008).
- [48] M. B. Gaarde and K. J. Schafer, in Attosecond Physics, edited by L. Plaja, R. Torres, and A. Zaïr (Springer Berlin Heidelberg, 2013).
- [49] M. B. Gaarde, C. Buth, J. L. Tate, and K. J. Schafer, Phys. Rev. A 83, 013419 (2011).
- [50] M. Wu, S. Chen, S. Camp, K. J. Schafer, and M. B. Gaarde, J. Phys. B 49, 062003 (2016).
- [51] R. R. Freeman, P. H. Bucksbaum, H. Milchberg, S. Darack, D. Schumacher, and M. E. Geusic, Phys. Rev. Lett. 59, 1092 (1987).

- [52] P. Agostini, P. Breger, A. L'Huillier, H. G. Muller, G. Petite, A. Antonetti, and A. Migus, Phys. Rev. Lett. 63, 2208 (1989).
- [53] C. Figueira de Morisson Faria, R. Kopold, W. Becker, and J. M. Rost, Phys. Rev. A 65, 023404 (2002).
- [54] Z. Chang, Fundamentals of attosecond optics (CRC Press, 2016).
- [55] M. B. Gaarde and K. J. Schafer, Phys. Rev. A 64, 013820 (2001).
- [56] J. Tate, T. Auguste, H. G. Muller, P. Salières, P. Agostini, and L. F. DiMauro, Phys. Rev. Lett. 98, 013901 (2007).
- [57] V. S. Yakovlev and A. Scrinzi, Phys. Rev. Lett. 91, 153901 (2003).
- [58] K. Schafer and K. Kulander, Laser Phys. 7, 740 (1997).
- [59] M. B. Gaarde and K. J. Schafer, Phys. Rev. A 62, 053411 (2000).
- [60] The slight disagreements between the 4s and 6s/4d resonant intensity and temporal structure might arise due to the states shifting less than ponderomotively, as has been previously observed in helium [23]. We will examine this in more detail as a function of wavelength below.
- [61] V. Strelkov, Phys. Rev. Lett. 104, 123901 (2010).
- [62] M. Tudorovskaya and M. Lein, Phys. Rev. A 84, 013430 (2011).
- [63] J. Feist, O. Zatsarinny, S. Nagele, R. Pazourek, J. Burgdörfer, X. Guan, K. Bartschat, and B. I. Schneider, Physical Review A 89, 033417 (2014).
- [64] S. Carlström, J. Preclíková, E. Lorek, E. W. Larsen, C. M. Heyl, D. Paleček, D. Zigmantas, K. J. Schafer, M. B. Gaarde, and J. Mauritsson, New J. Phys. 18, 123032 (2016).
- [65] M. Bellini, C. Lyngå, A. Tozzi, M. Gaarde, T. Hänsch, A. L'Huillier, and C.-G. Wahlström, Phys. Rev. Lett. 81, 297 (1998).
- [66] H. Merdji, M. Kovačev, W. Boutu, P. Salieres, F. Vernay, and B. Carré, Phys. Rev. A 74, 043804 (2006).
- [67] M. Murakami, J. Mauritsson, and M. Gaarde, Physical Review A 72, 023413 (2005).
- [68] C. Guo, A. Harth, S. Carlström, Y.-C. Cheng, S. Mikaelsson, E. Mårsell, C. M. Heyl, M. Miranda, M. Gisselbrecht, M. B. Gaarde, et al., Journal of Physics B: Atomic, Molecular and Optical Physics 51.
- [69] In [24], an α value close to π was measured for resonantly enhanced harmonic emission driven by a few-cycle pulse, indicating that the enhanced harmonic was in the cutoff region of the harmonic spectrum.